beyond the scope of the present work.

Summary

The second virial coefficient zero point (Θ-point) of traditional lattice polymers with nearest-neighbor pair interactions varies with the inverse square root of the chain length. We have succeeded in finding a unique solvent condition (Θ*-point) at which the second virial coefficients of the lattice polymers of various chain lengths vanish simultaneously. This was accomplished by associating an appropriate energy to each nearest-neighbor triplet in a polymer conformation. The Θ-point behavior of our lattice polymers is much like those of the continuous model polymers with two- and three-body δ-function interactions. On the other hand, the reduced moments of the lattice polymers at the Θ*-point are not Gaussian, in contrast to the continuous model polymers at the same point. Ignoring this last inconsistency, we have constructed a map providing the relations of the parameters of the two polymers, which were established from the consistency in the penetration function.

Acknowledgment. This work used the HITAC M-680H computer system in the Computer Center of the Institute of Molecular Science.

References and Notes

(1) Cherayil, B. J.; Douglas, J. F.; Freed, K. F. *J. Chem. Phys.* **1985**, *83*, 5293.

(2) Flory, P. J. *Principles of Polymer Chemistry*; Cornell University Press: New York, 1953.

(3) Bruns, W. *Macromolecules* **1984**, *17*, 2826.

(4) Janssens, M.; Bellemans, A. *Macromolecules* **1976**, *9*, 303.

(5) Watanabe, Y.; Katoh, M.; Okamoto, H. *Macromolecules*, in press.

(6) E.g.: Freed, K. F. *Renormalization Group Theory of Macromolecules*; Wiley: New York, 1987.

(7) E.g.: Hill, T. L. *Statistical Mechanics*; McGraw-Hill: New York, 1956.

(8) Wall, F. T.; Mandell, F. *J. Chem. Phys.* **1975**, *63*, 4592.

(9) Metropolis, N.; Rosenbluth, A. W.; Rosenbluth, M. N.; Teller, A. H.; Teller, E. *J. Chem. Phys.* **1953**, *21*, 1087.

(10) E.g.: Curro, J. G.; Schaefer, D. W. *Macromolecules* **1980**, *13*, 1199.

(11) Cherayil, B. J.; Douglas, J. F.; Freed, K. F. *J. Chem. Phys.* **1987**, *87*, 3089.

(12) de Gennes, P.-G. *Scaling Concepts in Polymer Physics*; Cornell University Press: Ithaca, NY, and London, 1979.

(13) Okamoto, H. *J. Chem. Phys.* **1988**, *88*, 5096.

(14) Oono, Y.; Freed, K. F. *J. Phys. A* **1982**, *15*, 1931.

(15) The penetration function R in this paper is connected with ψ in Oono and Freed's paper[14] by $R = 8(\pi^{3/2})\psi$.

(16) We found several misprints in numerical factors in Okamoto's paper.[13] In the 10th line on p 5103, -2ψ should be replaced by $-\psi/2$. In the 12th line on the same page, $-A_2/2\langle S^2\rangle^{3/2}$ should be replaced by $-2A_2/\langle S^2\rangle^{3/2}$. In the second line on p 5104, 2ψ should be replaced by $-\psi$ ($=R$).

(17) Freed, K. F. *J. Phys. A* **1985**, *18*, 871.

A Normal Vibrational Analysis of Syndiotactic Polystyrene

Nicholas M. Reynolds and Shaw Ling Hsu*

Polymer Science and Engineering Department, University of Massachusetts, Amherst, Massachusetts 01003

Received September 25, 1989; Revised Manuscript Received January 22, 1990

ABSTRACT: A normal vibrational analysis has been performed for the all-trans conformation of syndiotactic polystyrene. In this analysis a set of nonredundant symmetry coordinates and force constants has been employed for the phenyl ring. The other force constants needed for the chain have been transferred from studies of alkanes and have been applied to many polymers such as polyethylene and polypropylene. Observed infrared and Raman data, including polarization characteristics, have been satisfactorily assigned. Several localized ring modes that are also present in atactic and isotactic polystyrene as well as in toluene have been identified. Other conformation-sensitive features, which are unique to the syndiotactic isomer, are identified. Polarized infrared data show that coextruded samples have nearly perfect orientation of the trans sequences with the plane of the rings normal to the chain axis. The orientation is seen to increase upon annealing at 200 °C due to an increase in crystallinity. Upon higher temperature annealing a melting point of 285 °C is observed. The theoretical modulus is calculated from the slope of the dispersion curve of the longitudinal acoustic vibration near the Brillouin zone center. A value of 67 GPa was obtained.

Introduction

Recently, syndiotactic polystyrene (sPS) has been a subject of great interest.[1-9] Only quite recently has the synthesis been developed to produce nearly 100% syndiotactic polymer.[1,2,7] This material has several interesting physical characteristics: (1) a melting temperature of ca. 270 °C, although with annealing at gradually higher temperatures we have observed a melting point as high as 285 °C; (2) a variety of chain conformations, including a fully trans-planar zigzag backbone in addition to a helical conformation observed for solution-cast films; and (3) the presence of a solid–solid phase transition at ~190 °C involving changes in both chain conformation and packing.[1,3-7] Because of its inherent backbone stiffness and strong intermolecular interactions, macroscopic properties such as modulus and strength and their insensitivity to temperature are expected to exceed those of most polymers.

The structure of sPS is complex. Diffraction and spectroscopic studies have revealed that this polymer exists in a helical conformation upon casting from dilute solution and can easily transform to the all-trans conformation upon annealing or drawing.[3,5,6,10,11] The differences in the infrared and Raman spectra observed for different forms of sPS are striking. From the spectra obtained from samples of different tacticity and from pre-

* To whom correspondence should be addressed.

0024-9297/90/2223-3463$02.50/0

vious vibrational analyses of isotactic and atactic PS,[12-14] preliminary analyses have been carried out for sPS.[8,11] For example, infrared bands at 1222 or 538 cm^{-1} were found to be associated with the trans conformation, while features at 571, 934, and 943 cm^{-1} represent the helical structure.[3,11,15] These preliminary assignments have been useful to clarify the microstructures and their changes. However, the exact band assignments for sPS are still ill-defined. Therefore a normal vibrational analysis of sPS is necessary for a thorough analysis of the vibrational spectra in order to understand the microstructure and phase transition of this material.

A normal vibrational analysis for polystyrene is complicated because of the various cyclic and branching redundancies that exist and greatly increase the necessary number of internal coordinates needed for analysis. This overdefined set of coordinates is often used in order to take advantage of symmetry or to transfer force constants from one molecule to another. However, the use of a larger than necessary number of coordinates increases the number of force constants so that the set is indeterminant, and the eigenvalue solution may not be unique. Therefore the force constants lose physical meaning and cannot be easily refined or adapted to polystyrene and other polymers. It is also desirable to transfer well-developed force field sets calculated for small-ring molecules from first principles. In this study a set of force constants derived for a set of nonredundant symmetry coordinates is used for the phenyl ring, which were determined for benzene.[16] These coordinates have been applied in the analysis of substituted benzenes and also for poly(*p*-phenyleneterephthalamide).[17,18] One goal of this study is to determine the degree of coupling of the ring vibrations to the backbone modes and to correlate these bands with those that are sensitive to the all-trans conformation.

When the vibrational modes are well assigned, it is possible to calculate the theoretical modulus from the slope of the dispersion curve for the longitudinal acoustic mode (LAM) vibration at the zone center ($k = 0$). Such a calculation is performed for sPS. Since this calculation involves the vibrations of a single infinite chain, the presence of intermolecular interactions and their effect on the mechanical properties are unaccounted for. Therefore the value calculated represents a lower limit of the theoretical modulus.

Experimental Section

Polystyrene samples >99% syndiotactic (M_n = 125 000, M_w = 660 000) were obtained from Dow Chemical Co. Films were cast in aluminum pans from a 1% solution in chloroform and dried under vacuum. Oriented films with a draw ratio of 4 were obtained by solid-state coextrusion at 100 °C with the split-billet technique.[18] In this case the cast film was placed inside a high-density polyethylene billet. Polarized infrared spectra were obtained with a Bruker IFS 113v FTIR spectrometer equipped with a gold wire grid polarizer. Generally 200 scans were collected at 2-cm^{-1} resolution. Low-temperature infrared spectra were obtained in a liquid nitrogen cooled cell constructed in our laboratory. Polarized Raman measurements were made with a Jobin-Yvon U1000 spectrometer operating with a band-pass of 2 cm^{-1}. The highly polarized excitation radiation was the 5145-Å line of a Spectra Physics 165-08 argon ion laser providing 100 mW of power at the sample. A polarization scrambler, placed immediately following the analyzer, was used to remove intensity differences due to the anisotropic diffraction properties of the monochromator gratings. Two scattering geometries were employed for the polarized Raman measurements in order to correctly assign each vibration to a specific symmetry species. These are shown in Figure 1.

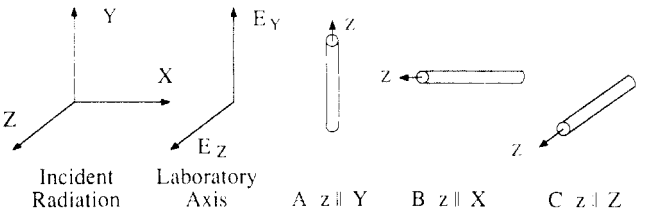

Figure 1. Schematic diagram of the sample orientation relative to the incident radiation for different scattering geometries.

Table I
Raman Scattering Activities for C_{2v} Symmetry

Scattering Geometry A

	symmetry species			
polarization	A_1	A_2	B_1	B_2
$X(YY)Z$	α_{xx}	0	0	0
$X(ZY)Z$	0	α_{xy}	α_{xz}	0
$X(YX)Z$	0	α_{xy}	α_{xz}	0
$X(ZX)Z$	α_{yy}, α_{zz}	0	0	α_{yz}

Scattering Geometry B

	symmetry species	
polarization	A_1	B_2
$X(YY)Z$	$(1/32)(12\alpha_{yy}^2 + 8\alpha_{yy}\alpha_{zz} + 12\alpha_{zz}^2)$	$(1/2)\alpha_{yz}^2$
$X(ZY)Z$	$(1/32)(4\alpha_{yy}^2 - 8\alpha_{yy}\alpha_{zz} + 4\alpha_{zz}^2)$	$(1/2)\alpha_{yz}^2$

Structure and Force Field

An all-trans planar structure was used for our vibrational analysis. This is the accepted structure for annealed sPS determined from diffraction and spectroscopic studies and conformational analyses.[1,3-11,20,21] Only limited structural information is available about the helical phase. The all-trans structure is simpler and should have higher mechanical properties. The factor group of the line group of the all-trans conformation of sPS is isomorphic with the C_{2v} point group. Vibrational modes are distributed among the symmetry species as follows: 29 A_1 ($\perp$), 17 A_2 (IR inactive), 17 B_1 ($\parallel$), and 29 B_2 ($\perp$). The modes are calculated for two values of the phase angle between oscillators of adjacent chemical repeats. The A_1 and B_1 symmetry species are associated with a phase angle of 0°, while the A_2 and B_2 symmetry species are associated with a phase angle of 180°.

Many of the band assignments can be made from polarized Raman measurements with highly oriented samples, although these measurements are complicated by the lack of perfect orientation and by the presence of multiple scattering from small crystallites (these films are not completely transparent). The assignment of symmetry species to specific incident and scattered polarization directions has been performed for C_{2v} symmetry.[22,23] The Raman scattering activities for the two geometries used are given in Table I. With geometry A, the $X(YY)Z$ polarization, with parallel incident and scattered radiation, gives the totally symmetric A_1 symmetry species. The $X(YX)Z$ or $X(ZY)Z$ polarizations are associated with the A_2 and B_1 species, while the $X(ZX)Z$ polarization gives the A_1 and B_2 symmetry species. Geometry B is needed to clearly distinguish between the A_1 and B_2 symmetry bands. As seen in Table I, the $X(YY)Z$ and $X(ZY)Z$ polarizations give identical scattering intensity for B_2 vibrations; however, the totally symmetric A_1 vibrations will have greater intensity for the $X(YY)Z$ polarization.

A schematic structure of sPS showing the internal coordinates is given in Figure 2. The indexing of the atoms for the internal coordinates is shown in Figure 3. The structural parameters and the internal coordinates are

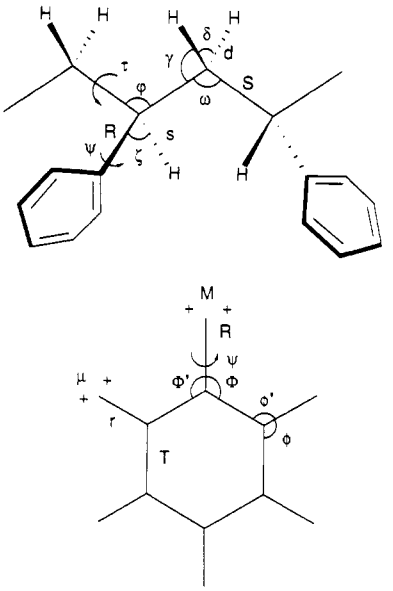

Figure 2. Schematic structure of sPS showing internal coordinates.

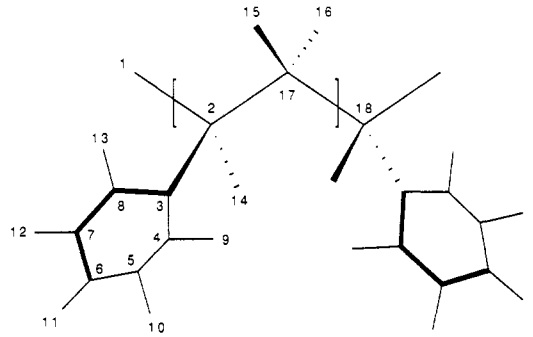

Figure 3. Schematic structure of sPS showing the indexing of atoms used for defining the internal coordinates.

Table II
Structural Parameters of All-Trans Syndiotactic Polystyrene[a]

length, Å	valence angle, deg	dihedral angle, deg
C–C = 1.397	∠(CCC) = 120	τ(CCCC) = 180
C–H = 1.084	∠(CCH) = 120	τ(CCCH) = 0
C–C′ = 1.51	∠(CCC′) = 120	τ(CCCC′) = 0
C′–C′ = 1.54	∠(C′C′C) = 109.47	τ(HCCC′) = 180
C′–H = 1.093	∠(CC′H) = 109.47	$\tau(C_3C'C'H_{16}) = 0$
	∠(C′C′H) = 109.47	$\tau(C_1C'C'C_{18}) = 0$
	∠(HC′H) = 109.47	$\tau(C_1C'C'H_{16}) = 120$
	∠(C′C′C′) = 109.47	$\tau(C_1C'C'H_{15}) = 240$

[a] C = ring carbon, C′ = chain carbon.

given in Tables II and III, respectively. In this calculation a set of nonredundant symmetry coordinates is employed for the phenyl ring.[16] A schematic diagram showing the atomic displacements for some of these coordinates is given in Figure 4. A list of the symmetry coordinates used in the calculation is given in Table IV. The force constants for the backbone chain were developed by Snyder and Schachtschneider for straight-chain and branched alkanes and have been applied to many polymers such as polyethylene and polypropylene.[24] Force constants for the phenyl ring were obtained from ab initio quantum chemical calculations on benzene.[16] Force constants describing the interaction of the ring with the backbone were taken from the work of La Lau and Snyder for substituted benzenes.[25] A complete list of the force constants used in this study is given in Table V. The vibrational analysis was performed with Wilson's GF

Table III
Definition of Internal Coordinates for Syndiotactic Polystyrene

Stretching

R_n	atoms	R_n	atoms
$R_1 = r(C'–C')$	(2,17)	$R_{10} = r(C–H)$	(4,9)
$R_2 = r(C'–C)$	(2,3)	$R_{11} = r(C–H)$	(5,10)
$R_3 = r(C'–H)$	(2,14)	$R_{12} = r(C–H)$	(6,11)
$R_4 = r(C–C)$	(3,4)	$R_{13} = r(C–H)$	(7,12)
$R_5 = r(C–C)$	(4,5)	$R_{14} = r(C–H)$	(8,13)
$R_6 = r(C–C)$	(5,6)	$R_{15} = r(C–H)$	(17,15)
$R_7 = r(C–C')$	(6,7)	$R_{16} = r(C–H)$	(17,16)
$R_8 = r(C–C)$	(7,8)	$R_{17} = r(C'–C')$	(17,18)
$R_9 = r(C–C)$	(8,3)		

Angle Bending

R_n	atoms	R_n	atoms
$R_{18} = \angle(C'C'H)$	(1,2,14)	$R_{33} = \angle(CCH)$	(7,8,13)
$R_{19} = \angle(C'C'C)$	(1,2,3)	$R_{34} = \angle(HCC)$	(13,8,3)
$R_{20} = \angle(C'C'C')$	(1,2,17)	$R_{35} = \angle(CCC')$	(8,3,2)
$R_{21} = \angle(H'C'C')$	(14,2,17)	$R_{36} = \angle(CCC)$	(3,4,5)
$R_{22} = \angle(CC'H)$	(3,2,14)	$R_{37} = \angle(CCC)$	(4,5,6)
$R_{23} = \angle(CC'C')$	(3,2,17)	$R_{38} = \angle(CCC)$	(5,6,7)
$R_{24} = \angle(C'CC)$	(2,3,4)	$R_{39} = \angle(CCC)$	(6,7,8)
$R_{25} = \angle(CCH)$	(3,4,9)	$R_{40} = \angle(CCC)$	(7,8,3)
$R_{26} = \angle(HCC)$	(9,4,5)	$R_{41} = \angle(CCC)$	(8,3,4)
$R_{27} = \angle(CCH)$	(4,5,10)	$R_{42} = \angle(C'C'C')$	(2,17,18)
$R_{28} = \angle(HCC)$	(10,5,6)	$R_{43} = \angle(C'C'H)$	(2,17,15)
$R_{29} = \angle(CCH)$	(5,6,11)	$R_{44} = \angle(C'C'H)$	(2,17,16)
$R_{30} = \angle(HCC)$	(11,6,7)	$R_{45} = \angle(HC'H)$	(15,17,16)
$R_{31} = \angle(CCH)$	(6,7,12)	$R_{46} = \angle(HC'C')$	(15,17,18)
$R_{32} = \angle(HCC)$	(12,7,8)	$R_{47} = \angle(HC'C')$	(16,17,18)

Out-of-Plane Bending

R_n	atoms	R_n	atoms
R_{48} = C–H opb	(4,9,5,3)	R_{51} = C–H opb	(7,12,8,6)
R_{49} = C–H opb	(5,10,6,4)	R_{52} = C–H opb	(8,13,3,7)
R_{50} = C–H opb	(6,11,7,5)	R_{53} = ring opb	(3,2,4,8)

Torsion

R_n	atoms	R_n	atoms
R_{54} = C′–C′ tor	(2,17)	R_{59} = C–C tor	(5,6)
R_{55} = C′–C′ tor	(17,18)	R_{60} = C–C tor	(6,7)
R_{56} = C–C′ tor	(3,2)	R_{61} = C–C tor	(7,8)
R_{57} = C–C tor	(3,4)	R_{62} = C–C tor	(8,3)
R_{58} = C–C tor	(4,5)		

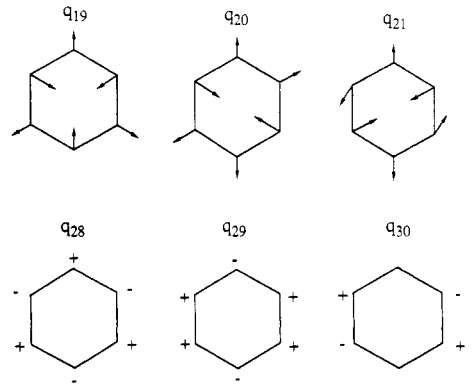

Figure 4. Definition of some of the nonredundant symmetry coordinates for the phenyl ring.

matrices with programs modified from Schachtschneider and Snyder's programs.[26] The calculated and observed frequencies along with the observed polarizations and calculated potential energy distribution are listed in Table VI.

Results and Discussion

The goal of this analysis is to predict the frequencies and potential energy distribution of the infrared- and

Table IV
Definition of Symmetry Coordinates for Syndiotactic Polystyrene

	notation	
C′–C′ str	S	$S_1 = R_1$
C′–C′ str		$S_2 = R_{17}$
C′–C str	R	$S_3 = R_2$
C–C str	T	$S_4 = R_4$
C–C str		$S_5 = R_5$
C–C str		$S_6 = R_6$
C–C str		$S_7 = R_7$
C–C str		$S_8 = R_8$
C–C str		$S_9 = R_9$
C′–H′ str	s	$S_{10} = R_3$
C′–H str	d	$S_{11} = R_{15}$
C′–H str		$S_{12} = R_{16}$
C–H str	r	$S_{13} = R_{10}$
C–H str		$S_{14} = R_{11}$
C–H str		$S_{15} = R_{12}$
C–H str		$S_{16} = R_{13}$
C–H str		$S_{17} = R_{14}$
C′C′H bend	ζ	$S_{18} = R_{18}$
HC′C′ bend		$S_{19} = R_{21}$
CC′H bend		$S_{20} = R_{22}$
C′C′C bend	φ	$S_{21} = R_{19}$
C′C′C′ bend		$S_{22} = R_{20}$
CC′C′ bend		$S_{23} = R_{23}$
C′C′C′ bend	ω	$S_{24} = R_{42}$
C′C′H bend	γ	$S_{25} = R_{43}$
C′C′H bend		$S_{26} = R_{44}$
HC′C′ bend		$S_{27} = R_{46}$
HC′C′ bend		$S_{28} = R_{47}$
HC′H bend	δ	$S_{29} = R_{45}$
C′CC bend	Φ	$S_{30} = R_{24}$
CCC′ bend	Φ'	$S_{31} = R_{35}$
C–H9 ipb	β	$S_{32} = (R_{26} - R_{25})/2^{1/2}$
C–H10 ipb		$S_{33} = (R_{28} - R_{27})/2^{1/2}$
C–H11 ipb		$S_{34} = (R_{30} - R_{29})/2^{1/2}$
C–H12 ipb		$S_{35} = (R_{32} - R_{31})/2^{1/2}$
C–H13 ipb		$S_{36} = (R_{34} - R_{33})/2^{1/2}$
C′–C ipb	β'	$S_{37} = (R_{24} - R_{35})/2^{1/2}$
trigonal def	q_{19}	$S_{38} = (R_{41} - R_{36} + R_{37} - R_{38} + R_{39} - R_{40})/6^{1/2}$
asym def A	q_{20}	$S_{39} = (2R_{41} - R_{36} - R_{37} + 2R_{38} - R_{39} - R_{40})/12^{1/2}$
asym def B	q_{21}	$S_{40} = (R_{36} - R_{37} + R_{39} - R_{40})/2$
C–H9 opb	μ	$S_{41} = R_{48}$
C–H10 opb		$S_{42} = R_{49}$
C–H11 opb		$S_{43} = R_{50}$
C–H12 opb		$S_{44} = R_{51}$
C–H13 opb		$S_{45} = R_{52}$
ring opb	M	$S_{46} = R_{53}$
puckering	q_{28}	$S_{47} = (R_{57} - R_{58} + R_{59} - R_{60} + R_{61} - R_{62})/6^{1/2}$
asym tor A	q_{29}	$S_{48} = (-R_{57} + R_{59} - R_{60} + R_{62})/2$
asym tor B	q_{30}	$S_{49} = (-R_{57} + 2R_{58} - R_{59} + R_{60} + 2R_{61} - R_{62})/12^{1/2}$
C′–C tor	Ψ	$S_{50} = R_{56}$
C′–C′ tor	τ	$S_{51} = R_{54}$
C′–C′ tor		$S_{52} = R_{55}$

Raman-active bands and to correlate these with the observed spectra for use in structural analysis. We are particularly interested in the assignments of bands that are sensitive to the all-trans chain conformation, which appears upon annealing at ~200 °C or upon drawing. Dramatic spectral changes are observed and are shown in Figure 5. Several localized modes assigned to ring vibrations are insensitive to the chain conformation. We are also interested in the degree of coupling of the ring to the backbone vibrations for the conformation-sensitive bands in comparison to isotactic polystyrene.

Polarized infrared spectra of coextruded and annealed sPS are shown in Figures 6–8. Polarized Raman spectra obtained with scattering geometry A are shown in Figures 9–11. Raman spectra obtained with geometry B are shown in Figures 12–14. Several localized ring vibrations may be assigned upon comparison of frequencies calculated for sPS with those for toluene. Some of these calculated bands are found at 1647, 1566, 1505, 1323, 1303, 1189, and 1163 cm^{-1}. These modes all involve ring CC stretching and CH in-plane bending, and many of these are also observed in atactic and isotactic polystyrene. The 1647- and 156l-cm^{-1} bands observed in the infrared at 1601 and 1584 cm^{-1}, respectively, have the same calculated frequencies in toluene. The agreement for these two bands is much less than satisfactory.[25] However, this result is consistent with an earlier study where the nonredundant force constants were applied.[18] These two bands show the worst agreement with the observed values aside from the CH stretching region, which has never been successfully analyzed. This region is shown in Figure 6, with all the CH stretching modes showing perpendicular polarization in the infrared.

The 1601- and 1584-cm^{-1} ring bands show high intensity for the *ZX* polarization for scattering geometry A and nearly identical intensity for the *YY* and *ZY* polarizations for geometry B and therefore belong to the B_2 symmetry species. In a previous analysis of atactic polystyrene, the 1601- and 1584-cm^{-1} bands were assigned to the B_1 and A_1 symmetry species. These assignments were

Table V
Force Constants for Syndiotactic Polystyrene

force constant	value	force constant	value
	(A) Chain		
K(d)	4.554	$F(S\omega)$	0.417
K(s)	4.588	$F(\gamma\omega)$	−0.031
K(R)	4.6813	$F(R\gamma)$	0.328
K(S)	4.337	$F(R\gamma')$	0.079
$H(\delta)$	0.550	$f_{\gamma\zeta'}$	0.127
$H(\gamma)$	0.655	$f_{\gamma\zeta}$	−0.005
$H(\zeta)$	0.657	$f_{\omega\varphi'}$	−0.011
$H(\omega)$	1.130	$f_{\omega\varphi}$	0.010
$H(\varphi)$	1.084	$f_{\gamma\varphi'}$	0.049
$H(\Psi)$	0.048	$f_{\gamma\varphi}$	−0.052
$H(\tau)$	0.072	$f_{\gamma\zeta''}$	0.002
$F(\delta)$	0.006	$f_{\gamma\zeta}$	0.009
F(SR)	0.101	$f_{\gamma\zeta''}$	−0.014
$F(\gamma)$	−0.021	$f_{\gamma\zeta'}$	−0.025
$F(\gamma')$	0.012	$F(\varphi)$	−0.041
	(B) Ring		
K(r)	5.176	$F(R_1\beta_1)$	0.167
K(R)	6.636	$R(R_1\beta_3)$	−0.010
$H(\beta)$	0.512	$F(R_1\beta_4)$	0.019
$H(\beta')$	0.7535	$F(R_1\beta')$	0.186
$H(q_{19})$	1.236	$F(R_1q_{20})$	0.134
$H(q_{20})$	1.236	$F(R_2q_{20})$	−0.268
$H(q_{21})$	1.236	$F(R_3q_{20})$	−0.067
$H(\gamma)$	0.5852	$F(r_2q_{21})$	−0.0857
$H(\gamma')$	0.6688	$F(r_3q_{21})$	0.0857
$H(q_{28})$	0.3763	$F(R_1q_{21})$	0.2321
$H(q_{29})$	0.3156	$F(R_3q_{21})$	−0.2321
$H(q_{30})$	0.3156	$F(\beta)^o$	0.009
$F(r)^o$	0.016	$F(\beta)^m$	−0.010
$F(r)^m$	0.005	$F(\beta)^p$	−0.001
$F(r)^p$	0.001	$F(\beta_2q_{20})$	−0.067
$F(r_1R_1)$	0.079	$F(\beta'q_{21})$	0.07736
$F(r_1R_2)$	−0.002	$F(\beta_2q_{21})$	−0.03863
$F(r_1R_3)$	−0.022	$F(\gamma)^o$	−0.092
$F(r_1\beta_2)$	0.005	$F(\gamma)^m$	−0.0004
$F(r_1\beta_3)$	−0.007	$F(\gamma)^p$	−0.0235
$F(r_1q_{19})$	0.105	$F(\gamma_1q_{28})$	−0.1681
$F(r_2q_{19})$	−0.105	$F(\gamma_2q_{28})$	0.1681
$F(Rq_{19})$	−0.105	$F(\gamma_1q_{29})$	−0.1700
$F(r_1q_{20})$	0.0495	$F(\gamma_2q_{29})$	0.085
$F(Rq_{20})$	−0.099	$F(\gamma_2q_{30})$	0.1472
$F(R)^o$	0.633	$F(\gamma_3q_{30})$	−0.1472
$F(R)^m$	−0.442	$F(R_1R)$	0.2506
$F(R)^p$	0.440	$F(R\beta')$	0.5415

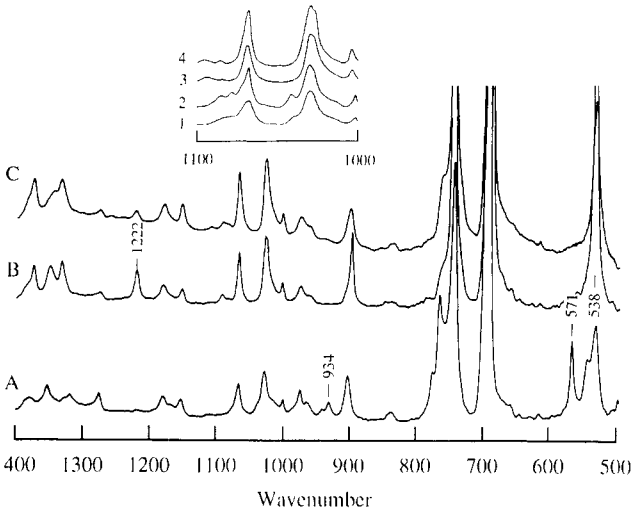

Figure 5. Infrared spectra of sPS: (A) solution-cast film; (B) after annealing at 295 °C for 0.5 h; (C) coextruded at 100 °C to a draw ratio of 4. Inset region: (1) cast film; (2) at liquid nitrogen temperature; (3) annealed at 200 °C for 1 h; (4) annealed at 200 °C and measured at liquid nitrogen temperature.

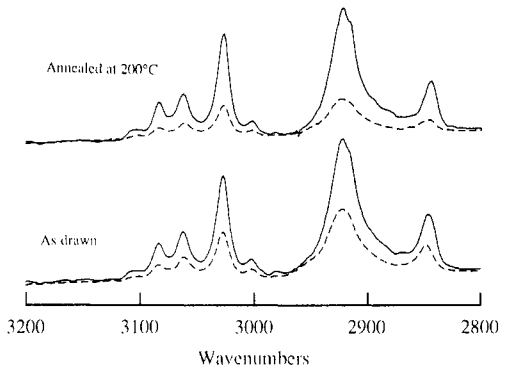

Figure 6. Polarized infrared spectra of coextruded sPS before and after annealing at 200 °C (3200–2800 cm^{-1}): perpendicular polarization (—); parallel polarization (- - -).

made based on the symmetry analysis of monosubstituted benzenes in which the substituent, which represents the chain backbone, has no symmetry. A C_2 symmetry axis exists along the 1 and 4 carbons of the ring. However, syndiotactic polystyrene has C_{2v} symmetry, with the C_2 axis bisecting the CH_2 group. Because of the different position of the symmetry axis compared to monosubstituted benzenes, many of the symmetry species assignments are different.

Modes calculated at 1505 and 1323 cm^{-1} and assigned to CH in-plane bending and CC stretching are close in frequency to the corresponding toluene bands at 1495 and 1327 cm^{-1}, respectively. The latter appears in the Raman spectrum of sPS at 1320 cm^{-1} and shows higher intensity for the XY polarization with geometry A, indicating it belongs to the B_1 or A_2 symmetry species. This band does not appear in the infrared, and since the A_2 species is infrared inactive for C_{2v} symmetry, the 1320-cm^{-1} band may be tentatively assigned to the A_2 species.

Chain backbone vibrations are usually found in the 900–1200 cm^{-1} region, and here substantial differences are seen in the spectra for different tacticities. One unique feature for sPS is the 1222-cm^{-1} band, which shows strong parallel polarization. It does not appear for the atactic and isotactic isomers. This band has a transition dipole moment parallel to the chain axis, as seen from the parallel polarization shown in Figure 7, and is present only upon annealing or drawing. Therefore it is due to a sequence of trans conformations. It is assigned to CCH

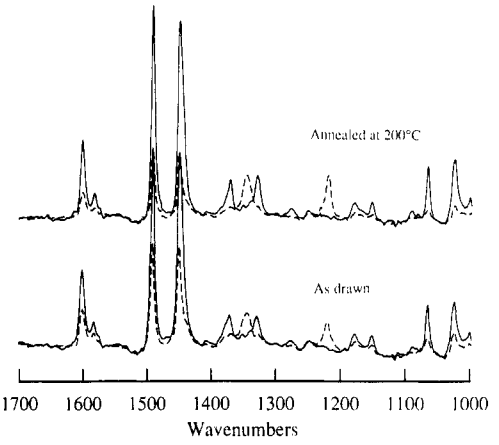

Figure 7. Polarized infrared spectra of coextruded sPS before and after annealing at 200 °C (1700–1000 cm^{-1}): perpendicular polarization (—); parallel polarization (- - -).

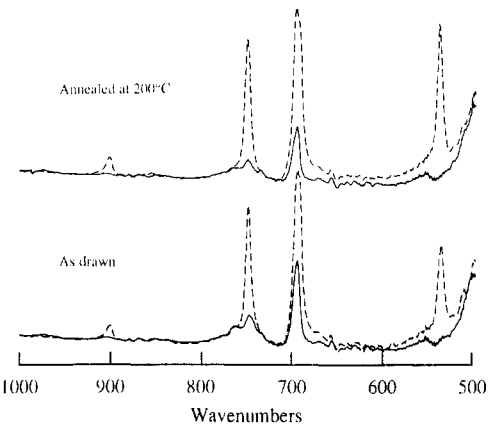

Figure 8. Polarized infrared spectra of coextruded sPS before and after annealing at 200 °C (1000–500 cm^{-1}): perpendicular polarization (—); parallel polarization (- -).

bending of the CH_2 and CH groups and CC backbone stretching, and belongs to the B_1 symmetry species.

Several of the bands that are sensitive to chain conformation involve coupling of the ring vibrations to the backbone modes. The 1376-cm^{-1} band appears strongly in the Raman for the YY polarization for geometry A and belongs to the A_1 symmetry species. It is assigned to CCH backbone bending, CH in-plane bending, and CC′ and CC stretching. It appears with strong intensity in the infrared for the all-trans form. A mode observed at 1205 cm^{-1} in the Raman shows highest intensity for the ZX polarization with scattering geometry A and for the YY polarization with geometry B. Thus it belongs to the A_1 symmetry species. It is tempting to assign this band to that calculated at 1210 cm^{-1}; however, this band is calculated with a phase angle of 180° and therefore must belong to the A_2 or B_2 symmetry species.

In this region nearly all vibrations involve ring CC stretching and CH in-plane bending. The 1028-cm^{-1} band is assigned to these modes as well as the trigonal ring deformation. From its higher Raman intensity for the YY polarization (geometry B), it is assigned to the A_1 symmetry species. As shown in Figure 5, at liquid nitrogen temperature this band splits into two components. This was seen previously[11] and suggests the presence of crystal field splitting, indicating that this band is particularly sensitive to chain packing. However, there are bands calculated at 1024 and 1031 cm^{-1}, which involve the ring and backbone, respectively. It is more likely that it is these features, which are more clearly resolved at low temperature, which are present rather than crystal field

Table VI
Observed and Calculated Frequencies (cm^{-1}) and Potential Energy Distribution of sPS

IR	pol	Raman	sym species	calcd	pot energy dist
				3092	r(99)
				3092	r(99)
3083	⊥			3081	r(100)
				3081	r(100)
				3071	r(100)
				3071	r(100)
3062	⊥	3062		3062	r(100)
				3062	r(101)
		3055		3054	r(100)
				3054	r(101)
				2929	d(95)
2922	⊥			2928	d(100)
		2906		2905	s(98)
				2903	s(95)
2846	⊥	2849		2856	d(100)
				2855	d(99)
				1647	T(74), β(17), q_{20}(6), q_{21}(5), R(5)
1601	⊥	1604	B_2	1647	T(74), β(17), q_{20}(6), q_{21}(5), R(5)
				1566	T(86), β(21), q_{20}(6), q_{21}(5)
1583	⊥	1584	B_2	1566	T(86), β(21), q_{20}(6), q_{21}(5)
1493	⊥			1505	β(52), T(38), R(9)
				1503	β(55), T(38), R(8)
				1459	δ(49), β(22), γ(15), T(12)
1452	⊥	1454	B_2	1454	β(56), T(34)
				1453	β(77), γ(21)
				1450	β(38), δ(27), T(23), γ(7)
1376	⊥	1375	A_1	1370	γ(29), β(28), ζ(22), R(15), T(8)
				1358	β(46), ζ(30), T(13), R(12), S(6)
1347	∥	1347	B_1	1357	ζ(42), γ(43), S(42)
1334	⊥	1331	B_2	1330	ζ(64), γ(18), S(6)
				1323	β(74), T(13), γ(12)
		1320	A_2	1323	γ(58), β(25), T(8), S(8), ζ(7)
				1311	T(76), β(36), γ(28)
		1303	A_1	1303	T(136), β(18), γ(9)
1279	⊥		B_2	1279	T(69), R(19), β(18), γ(14), φ(5)
1253	⊥			1237	R(23), β(12), ζ(12), S(11), T(10), γ(9), q_{19}(8), ω(5), φ(5)
1222	∥	1222	B_1	1235	γ(54), ζ(45), S(7)
		1205	A_1	1210	ζ(34), R(14), T(14), β(12), q_{19}(9), γ(8)
				1189	β(80), T(9)
1181	⊥	1182	B_2	1189	β(78), T(10)
				1163	β(79), T(15)
				1163	β(80), T(17)
1155	⊥	1156	B_2	1156	γ(73), ζ(19), S(14)
				1154	ζ(52), T(17), γ(25), β(8), S(8)
1092	⊥			1091	S(58), γ(23) φ(13)
				1084	T(28), β(26), S(17), γ(11)
				1080	S(32), ω(14), φ(13), q_{19}(8), γ(6), β(6)
1069	⊥	1072		1065	T(50), β(32)
				1049	S(42), T(26), β(11), γ(9)
				1031	S(76), ζ(11), γ(8), φ(5)
				1024	T(52), β(20), q_{19}(12)
1028	⊥	1031	A_1	1021	T(49), q_{19}(21), β(16)
				990	q_{19}(47), T(46)
1004	⊥	1002	A_1	990	q_{19}(57), T(35)
				982	μ(136), q_{28}(29)
				982	μ(135), q_{28}(28)
				976	γ(27), T(25), ζ(16), S(14), q_{19}(5)
				964	μ(126), q_{30}(12)
				964	μ(126), q_{30}(12)
901	∥		B_1	911	μ(117), q_{28}(14), q_{29}(9), M(8)
				909	μ(120), q_{28}(13), q_{29}(9), M(7)
				854	γ(64), ζ(14), φ(5), μ(6)
				839	μ(113)
				839	μ(113)
				776	q_{28}(83), μ(43), M(31)
		773	A_1	760	R(26), T(23), q_{20}(25), q_{19}(11), φ(5)
750	∥		B_1	759	q_{28}(86), μ(52), M(28), γ(11)
				751	q_{20}(26), R(22), T(21), q_{19}(9), γ(8), φ(5)
				697	μ(101), q_{28}(49)
695	∥		B_1	696	μ(94), q_{28}(61)
		622	B_2	626	q_{21}(80)
				622	q_{21}(87)
				610	q_{28}(44), ω(32), μ(18), φ(19), q_{29}(8), ζ(7), S(6)
				556	q_{20}(40), φ(29), R(11), Φ(9), T(6)
				548	φ(37), q_{20}(33), q_{21}(9), ζ(7), γ(6), Φ(6)

Table VI (Continued) Observed and Calculated Frequencies (cm^{-1}) and Potential Energy Distribution of sPS

IR	pol	Raman	sym species	calcd	pot energy dist
538	‖		B_1	536	$q_{29}(52)$, $q_{28}(30)$, M(28), $\mu(23)$, $\varphi(20)$
		525	B_2	508	$\varphi(26)$, $\gamma(20)$, $q_{20}(19)$, $\zeta(14)$, R(14), $\Phi(12)$, $\tau(7)$
				465	$q_{29}(86)$, M(37), $\omega(26)$
		403	A_1	402	$q_{30}(159)$, $\mu(28)$
				402	$q_{30}(159)$, $\mu(28)$
				396	$\Phi(27)$, $q_{20}(25)$, $\varphi(15)$, T(7)
				327	$q_{29}(78)$, $\varphi(37)$, M(10), $\mu(9)$, $\tau(7)$
		232		257	$\varphi(53)$, $q_{20}(12)$, R(9), S(6)
				207	$q_{29}(58)$, $\varphi(16)$, $\omega(16)$, $\mu(14)$, M(5), $q_{28}(5)$
				201	$\Phi(77)$, $\varphi(15)$, $\zeta(8)$, R(6)
		177	A_1	177	$\tau(36)$, M(27), $q_{29}(20)$, $\mu(10)$
				144	$\Phi(57)$, $\varphi(19)$, R(14), $\zeta(9)$, $\tau(6)$
				46	$\tau(38)$, M(24), Z(16), $\varphi(14)$
				40	M(45), $\varphi(42)$, $\omega(8)$
				36	Z(93)
				35	Z(79), $\tau(16)$
				20	$\tau(91)$

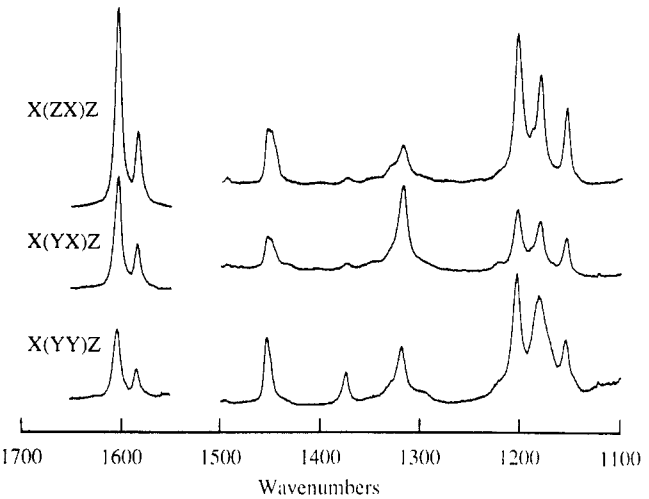

Figure 9. Polarized Raman spectra (scattering geometry A) of coextruded sPS after annealing at 210 °C for 3 h (1700–1100 cm^{-1}).

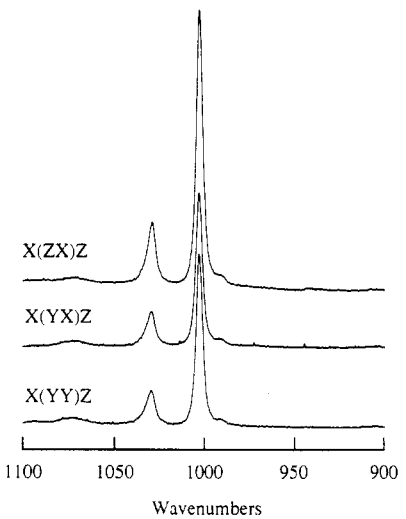

Figure 10. Polarized Raman spectra (scattering geometry A) of coextruded sPS after annealing at 210 °C for 3 h (1100–900 cm^{-1}).

splitting. The 1002-cm^{-1} Raman band, calculated at 990 cm^{-1}, is assigned to the ring trigonal deformation and CC stretching. It appears with highest intensity for the *ZX* polarization for geometry A and for the *YY* polarization for geometry B and is therefore an A_1 mode.

An intense Raman-active band is observed at 773 cm^{-1}. It shows higher intensity for the *YY* polarization with geometry B and is therefore assigned to the A_1 symmetry species band at 760 cm^{-1}. This band is a mixed mode involving the CC′ stretching, ring CC stretching, and ring trigonal and asymmetric deformation. It also appears in the toluene calculation at 783 cm^{-1} with the same assignment. A similar band is observed at 785 cm^{-1} for isotactic polystyrene, although this mode was also assigned to CCH bending of the CH_2 group.[13]

In the region below 1000 cm^{-1} there are several ring vibrations associated with the CH out-of-plane bending and the ring torsions. These are located at 901, 750, 695, and 538 cm^{-1}. The observed frequencies agree well with the calculated frequencies of 911, 759, 696, and 536 cm^{-1}. These bands all exhibit parallel polarization in the infrared spectrum, as seen in Figure 8, and are assigned to

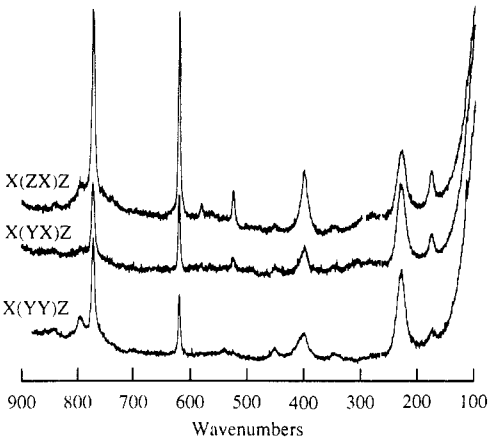

Figure 11. Polarized Raman spectra (scattering geometry A) of coextruded sPS after annealing at 210 °C for 3 h (900–100 cm^{-1}).

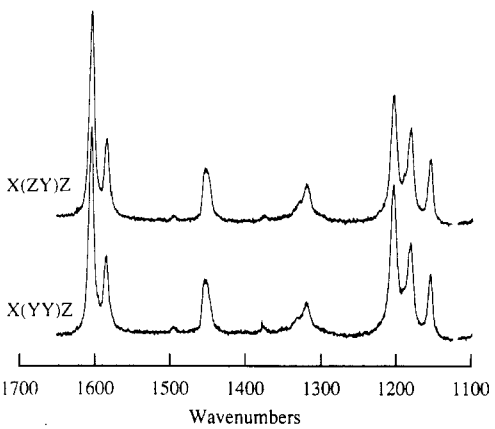

Figure 12. Polarized Raman spectra (scattering geometry B) of coextruded sPS after annealing at 210 °C for 3 h (1700–1100 cm^{-1}).

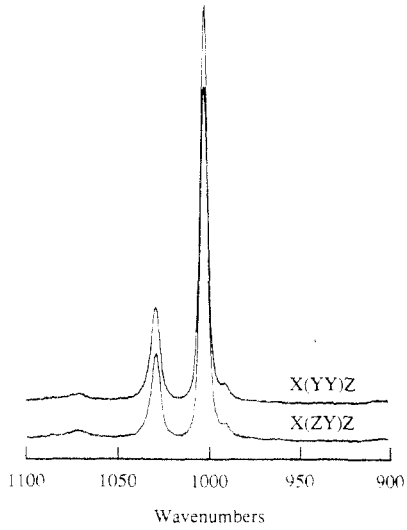

Figure 13. Polarized Raman spectra (scattering geometry B) of coextruded sPS after annealing at 210 °C for 3 h (1100–900 cm^{-1}).

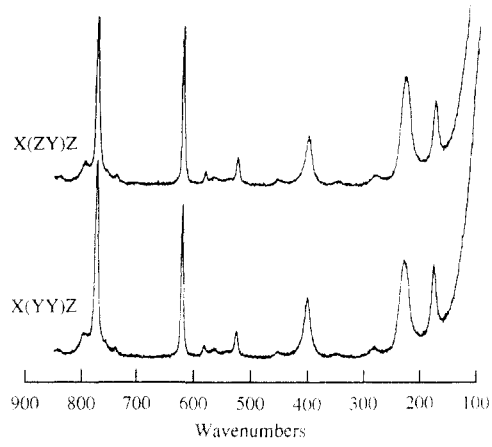

Figure 14. Polarized Raman spectra (scattering geometry B) of coextruded sPS after annealing at 210 °C for 3 h (900–100 cm^{-1}).

the B_1 symmetry species. Similar bands are found in isotactic and atactic polystyrene. The 538-cm^{-1} band has been assigned previously from studies of model polystyrene compounds to the ν_{16b} out-of-plane ring mode located in trans sequences of four or more units long.[15] In isotactic polystyrene, bands in this region contain out-of-plane bending of the ring,[12,13] and this is also seen in the 538-cm^{-1} band. In our previous study, this band showed increased intensity upon annealing or drawing, confirming that it is due to a long sequence of trans isomers.[11] Another band observed at 571 cm^{-1} for a cast film was concluded to correspond to this same mode for a structure containing gauche conformations. The 538-cm^{-1} band shows intensity only for the parallel polarization, with complete extinction for perpendicular polarization. Therefore the trans sequences have nearly perfect orientation, and since the transition dipole moment of this out-plane-ring vibration should be nearly perpendicular to the ring, the rings must be perpendicular to the chain axis. This has been suggested by previous experimental and theoretical studies.[4,20,21] In toluene, the corresponding bands are seen at lower frequencies: 901, 730, and 693 cm^{-1}. There is no corresponding band in toluene for the 538-cm^{-1} band of sPS. This is probably due to the absence of the backbone bending component for toluene. This coupling also gives this band its sensitivity to chain conformation. Another out-of-plane ring mode is the 622-

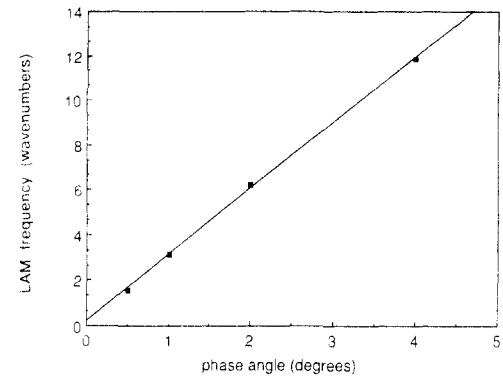

Figure 15. Dispersion curve of the longitudinal acoustic branch.

cm^{-1} band which appears strongly for the *ZX* polarization in the Raman (geometry A) and belongs to the B_2 symmetry species. This band also appears in the toluene calculation. It is insensitive to tacticity and appears in atactic polystyrene at 621 cm^{-1}.

Vibrational modes in the low-frequency region below 600 cm^{-1} are more delocalized and are much more difficult to assign. However, based on the polarized Raman spectra some of these bands may be assigned. Bands in this region, with the exception of the 403-cm^{-1} ring mode, all involve significant coupling of the chain to the backbone vibrations. This has also been observed for isotactic PS in which these vibrations are also highly conformation sensitive. A weak Raman band is observed at 527 cm^{-1} with *ZX* polarization (geometry A), and with equal intensity for *YY* and *ZY* polarization (geometry B), and is therefore assigned to the B_2 symmetry species. This band involves coupling of the ring to the backbone and is predominantly backbone skeletal and CCH bending and also ring asymmetric torsion.

A band observed at 403 cm^{-1} is assigned to ring asymmetric torsion and CH out-of-plane bending and agrees well with the calculated frequency of 402 cm^{-1}. This band shows slightly greater intensity for the ZX polarization and is assigned to the B_2 symmetry species. This localized ring mode appears at 401 cm^{-1} in the toluene calculation and is also seen in atactic and isotactic PS. A broad intense Raman band observed at 232 cm^{-1} may correspond to the mode calculated at 257 cm^{-1} involving coupling of the backbone bending and asymmetric torsion, along with chain CC and CC′ ring–chain stretching. It does not show significant polarization. Finally, a band appears at 177 cm^{-1}, showing greater intensity for *ZX* polarization (geometry A) and for *YY* polarization (geometry B), thus belonging to the A_1 symmetry species. For isotactic polystyrene a band is observed at 225 cm^{-1} involving ring in-plane bending,[13] which agrees with the present assignment for the 177-cm^{-1} band in sPS.

Conformation-Sensitive Bands. As shown in Figure 5, significant changes in the infrared spectra occur upon annealing near 200 °C or drawing a cast film, indicating a change in the chain conformation and packing of the molecules. Several bands disappear such as the 943-, 934-, 769-, 571-, and 548-cm^{-1} bands in the infrared and the 800-cm^{-1} band in the Raman. Other features appear such as the 1376-, 1334-, 1222-, and 548-cm^{-1} bands. We have observed these frequency values in the calculated results. The 1376-, 1334-, 1222-, and 548-cm^{-1} infrared bands, which show increased intensity upon annealing or coextrusion, can be correlated well with the calculated values. As previously stated, the 1376-, and 548-cm^{-1} bands involve coupling of the ring to the backbone, while the 1334- and 1222-cm^{-1} bands are only associated with the chain backbone. Also appearing with

drawing or annealing is the weak 1092-cm^{-1} infrared skeletal band. Some of the bands associated with the helical phase at 943, 934 (infrared), and 800 (Raman) cm^{-1} are not reproduced in the calculation. This supports the conclusion that these bands are not associated with the all-trans conformation but with a structure containing gauche conformations.

The polarized infrared spectra in Figures 6–8 show a significant increase in dichroism upon annealing the free-standing film at 200 °C. Thus the overall segmental orientation increases even if the film is annealed without tension. This phenomenon is very interesting since polyethylene shows a reduction in the overall orientation when annealed due to the relaxation of the amorphous regions.[27] Increases in orientation with annealing have also been observed for polypropylene and blends of poly(vinylidene fluoride) with poly(methyl methacrylate).[28,29] The increase in orientation for sPS is most likely also due to an increase in crystallinity upon annealing the drawn film. The crystalline orientation must be significantly higher than the amorphous orientation, and therefore an increase in crystallinity should increase the overall orientation. It is not yet known how the amorphous orientation changes with annealing.

Modulus Calculation. Since the mechanical properties of sPS have yet to be reported, a determination of the theoretical modulus is desirable. Using the elastic rod model, one may determine the modulus E from the frequency of the longitudinal acoustic branch by the relationship

$$\nu = \frac{1}{2cL}\left[\frac{E}{\rho}\right]^{1/2} \quad (1)$$

where L is the chain length, ρ is the density, and c is the speed of light. Strictly speaking, this calculation is only applicable to a chain of finite length L. However, we have calculated the acoustic branch by varying the phase angle of the equivalent vibration located at adjacent chemical repeats at ca. 0.5° increments from 0.5° to 4°. This phase angle is inversely proportional to the wavelength or the equivalent chain length, 875–112 Å, respectively.[30] In this fashion we can obtain the LAM frequency of various chain lengths, although the calculations are associated with an infinite chain. The density value of 1.00 g/cm^3 is determined from the crystal structure of Greis et al.[4] A plot of the LAM dispersion curve is given in Figure 15. From the slope of this dispersion curve, a modulus value of 67 GPa is calculated. No theoretical or experimental modulus values have been reported as of yet. This value is based on the vibrational analysis of a single chain. Therefore the effects of intermolecular interactions, which would raise the modulus, are not accounted for, and this modulus value represents a lower limit. These interactions should be significant given the structure of Greis et al., consisting of a superstructure of clusters of three chains with overlapping of the phenyl rings. Such intermolecular interactions would produce a higher modulus value. However, the calculated value shown in this study, the lower limit, should provide a basis value for further investigations. This value is significantly lower than the value calculated for polyethylene of ca. 300 GPa. This is because the cross-sectional area of a polystyrene chain is significantly larger than that of a polyethylene chain due to the phenyl rings. We have used Treloar's method in our previous calculation without much success.[18] When a reliable force field is available, normal vibrational analysis is the preferred method.

Conclusions

In this study a normal vibrational analysis has been performed for the trans-planar form of syndiotactic polystyrene. A set of nonredundant symmetry coordinates was employed for the phenyl ring. No refinement has been made on the force constant set, yet the calculated frequencies agree well with the observed bands, including polarization characteristics. Upon comparison with calculations on toluene, several localized conformation-insensitive ring modes are identified. Comparison with the spectra of atactic and isotactic PS and previous normal coordinate analyses on isotactic PS shows features that are unique to the all-trans structure of sPS. Bands such as the 1222-cm^{-1} band which only appear for the syndiotactic isomer in an annealed or drawn sample are identified in the calculation. Several bands involve significant coupling of the backbone and ring vibrations, and some of these such as the 1374- and 538-cm^{-1} bands are sensitive to chain conformation.

Large intensity changes are observed upon annealing or drawing cast films, and several bands that are removed upon heating or drawing such as the 943- and 934-cm^{-1} infrared bands and the 800-cm^{-1} Raman band are not reproduced by the calculation. This provides good evidence that these bands are representative of gauche conformations.

Solid-state coextrusion was found to be an effective method to produce highly oriented films for polarization studies. The high dichroism of the 1222-cm^{-1} skeletal band and the 538-cm^{-1} ring mode, both of which are sensitive to trans conformations, suggests that the trans sequences have nearly perfect orientation. As the 538-cm^{-1} band is an out-of-plane ring mode, the complete parallel polarization proves that the plane of the rings lies perpendicular to the chain axis, in agreement with previous studies. Annealing the freely standing drawn film results in a substantial increase in the segment orientation. This orientation increase is thought to be due to the increase in crystallinity that occurs upon annealing.

The theoretical modulus has been calculated from the slope of the dispersion curve of the longitudinal acoustic branch near the Brillouin zone center at which the vibrations of adjacent repeat units are moving in phase. A value of 67 GPa was obtained.

Acknowledgment. The financial support of a grant from the National Science Foundation, Polymers Program, Grant No. DMR 8919-105 (S.C.H.), is deeply appreciated. We also thank Dow Chemical for providing the syndiotactic polystyrene samples used in this study.

References and Notes

(1) Ishihara, N.; Seimiya, T.; Kuramoto, M.; Uoi, M. *Macromolecules* **1986**, *19*, 2464.
(2) Zambelli, A.; Longo, P.; Pellecchia, C.; Grassi, A. *Macromolecules* **1987**, *20*, 2035.
(3) Kobayashi, M.; Nakaoki, T.; Uoi, M. *Polym. Prepr., Jpn.* **1988**, *37*, E432.
(4) Greis, O.; Xu, Y.; Asano, T.; Petermann, J. *Polymer* **1989**, *30*, 590.
(5) Immirizi, A.; de Candia, F.; Iannelli, P.; Zambelli, A. *Makromol. Chem., Rapid Commun.* **1988**, *9*, 761.
(6) Vittoria, V.; de Candia, F.; Iannelli, P.; Immirizi, A. *Makromol. Chem., Rapid Commun.* **1988**, *9*, 765.
(7) Ishihara, N.; Kuramoto, M.; Uoi, M. *Macromolecules* **1988**, *21*, 3356.
(8) Conti, G.; Santoro, E.; Resconi, L.; Zerbi, G. *Mikrochim. Acta* **1988**, *1*, 297.
(9) Nyquist, R. A. *Appl. Spectrosc.* **1989**, *43*, 440.
(10) Petermann, J., private communication.

(11) Reynolds, N. M.; Savage, J. D.; Hsu, S. L. *Macromolecules* **1989**, *22*, 2867.
(12) Painter, P. C.; Koenig, J. L. *J. Polym. Sci., Polym. Phys. Ed.* **1977**, *15*, 1885.
(13) Snyder, R. W.; Painter, P. C. *Polymer* **1981**, *22*, 1633.
(14) Liang, C. Y.; Krimm, S. *J. Polym. Sci.* **1958**, *27*, 241.
(15) Jasse, B.; Monnerie, L. *J. Mol. Struct.* **1977**, *39*, 165.
(16) Pulay, P.; Fogarasi, G.; Boggs, J. E. *J. Chem. Phys.* **1981**, *74*, 3999.
(17) Kim, P. K.; Hsu, S. L.; Ishida, H. *Macromolecules* **1985**, *18*, 1905.
(18) Kim, P. K.; Chang, C.; Hsu, S. L. *Polymer* **1986**, *27*, 34.
(19) Zachariades, A. E.; Mead, W. T.; Porter, R. S. *Chem. Rev.* **1980**, *80*, 351.
(20) Yoon, D. Y.; Sundararajan, P. R.; Flory, P. J. *Macromolecules* **1975**, *8*, 776.
(21) Doherty, D. C.; Hopfinger, A. J. *Macromolecules* **1989**, *22*, 2472.
(22) Wilson, E. B., Jr.; Decius, J. C.; Cross, P. G. *Molecular Vibrations: The Theory of Infrared and Raman Vibrational Spectra*; Dover: New York, 1980; p 325.
(23) Schlotter, N. E.; Rabolt, J. F. *Polymer* **1984**, *25*, 165.
(24) Snyder, R. G.; Schachtschneider, H. H. *Spectrochim. Acta* **1965**, *21*, 169.
(25) La Lau, C.; Snyder, R. G. *Spectrochim. Acta* **1971**, *27A*, 2073.
(26) Schachtschneider, H. H.; Snyder, R. G. *Spectrochim. Acta* **1963**, *19*, 117.
(27) Peterlin, A. *Colloid Polym. Sci.* **1987**, *265*, 357.
(28) Samuels, R. J. *J. Polym. Sci., Polym. Phys. Ed.* **1979**, *17*, 535.
(29) Kaufmann, W.; Petermann, J.; Reynolds, N.; Thomas, E. L.; Hsu, S. L. *Polymer*, in press.
(30) Snyder, R. G.; Schachtschneider, J. H. *Spectrochim. Acta* **1963**, *19*, 85.

Registry No. sPS, 28325-75-9.

Diffusion in Quasi Two-Dimensional Macromolecular Solutions

P. Eggl,[‡] D. Pink,*[,†] B. Quinn,[†] H. Ringsdorf,[§] and E. Sackmann[‡]

Theoretical Physics Institute, St. Francis Xavier University, Antigonish, Nova Scotia, Canada B2G 1C0, Physik Department, Biophysik Group, Technische Universität, München, D-8046, Garching, FRG, and Institut für Organische Chemie, Universität Mainz, Mainz, D-6500, FRG

Received May 1, 1989; Revised Manuscript Received December 13, 1989

ABSTRACT: Membranes composed of a linearly polymerized amphiphile (with molecules interconnected via functional groups attached to the head groups via spacers) and dimyristoylphosphatidylcholine (DMPC) were studied in order to test their usefulness as models of two-dimensional macromolecular solutions. For that purpose a comparative experimental and Monte Carlo simulation study of the lateral diffusion of monomeric tracers and the self-diffusion of macrolipids was performed. Measurements of the diffusion coefficients were performed by the photobleaching technique in giant vesicles and in asymmetric bilayers supported on argon-sputtered glass substrates, with the inner (proximal) monolayer being composed of DMPC and the outer (distal) of the macromolecular solution. In the former case polymerization was performed by UV (285-nm) excitation and carried out chemically in the latter by using a hydrophilic initiator. The hydrodynamic radii of the photochemically and chemically polymerized macrolipids were obtained from the self-diffusion coefficients (of the macrolipids) by the application of a recent theory of diffusion in membranes in frictional contact with solid surfaces. The friction is transmitted by a thin lubricating water film (of some 10-Å thickness) between the proximal monolayer and the solid surface and can lead to a strong dependence of the diffusion coefficient on the size of the diffusant. We found a ratio of the radii of the macrolipid (a_p) to the monomer (a_m) of $a_p/a_m \approx 7$ for the photochemically polymerized species and of $a_p/a_m \approx 70$ for the chemically polymerized species. By assuming that the 2D mean-square radius of gyration scales as $N^{3/4}$, we obtained a degree of polymerization of $N = 20$ for the former and of $N = 300$ for the latter case showing that chemical polymerization is essential for the preparation of large macrolipids. Monte Carlo simulations in order to calculate the diffusion coefficients of monomeric tracers and macrolipids were carried out for fractions of area covered by the macromolecules varying from 10% to 80%. Two polymer conformations, representing extreme cases, were considered: a collapsed two-dimensional coil and an extended chain. The best agreement was found to be between experimental and simulated diffusion coefficients obtained for a linear combination of the collapsed and extended chain models, with the probability of the polymers to be in their collapsed states being about 0.4. The comparison suggests a value of $N \approx 24$ for the degree of polymerization of the photochemically polymerized species in good agreement with the experimental value.

I. Introduction

Membranes composed of monomeric lipids and polymerized amphiphiles (called macrolipids in this paper) are becoming of great interest. Some examples of their practical applications are (1) the development of drug delivery systems,[1] (2) the stabilization of Langmuir–Blodgett films, and (3) the mimicking (simulation) of cell surfaces.[1b,2] In addition, polymerized membranes offer new possibilities to prepare low-dimensionality macromolecular solutions or gels in order to study their fundamental properties, such as scaling laws, configurations, and polymerization processes in two dimensions.

In the present work we report combined experimental and Monte Carlo simulation studies of the lateral diffusion of monomolecular and macromolecular species in quasi two-dimensional solutions of (linear) macromolecular lip-

† St. Francis Xavier University.
‡ Technische Universität.
§ Universität Mainz.

0024-9297/90/2223-3472$02.50/0